A Multi-Motor Architecture for Electric Vehicles

Omar Nezamuddin, Rishikesh Bagwe, and Euzeli dos Santos Jr.
Department of Electrical and Computer Engineering
Purdue School of Engineering and Technology
Indianapolis, Indiana 46202
onezamud@iupui.edu, rbagwe@iupui.edu, eudossan@iupui.edu

***Abstract*—This paper proposes an architecture for EVs with three or more electric motors and highlights when adding more motors does not impact the battery state of charge (SOC). The proposed control algorithm optimizes the use of the motors on-board to keep them running in their most efficient regions. Simulation results along with a comparison with other current motors used in EVs is presented in this paper, and further discussion on the results is presented. With this architecture, the powertrain would see a combined efficiency map that incorporates the best operating points of the motors. Therefore, the proposed architecture will allow the EV to operate with a higher range for a given battery capacity.**

I. Introduction

In recent years, the automotive industry has been inclined to shift from powertrains with only internal combustion engines (ICEs) to either an ICE combined with an electric motor (HEVs) or electric motors only (EVs). The two main driving factors are the reduction of carbon dioxide (CO_2) emission and the increase in the price of fuel. HEVs have a more complex powertrain when compared to EVs, and plenty of propulsion architectures have been proposed for the use in HEVs [1]. The three main types are parallel HEV, series HEV, and a series-parallel HEV. The series-parallel HEV system is more complex than the other two configurations, its main advantage is that it can allow the ICE to run closer to its higher efficiency regions more often [2].

Electric vehicles, on the other hand, couples an electric motor to axle and wheels through transmission/differential and a power electronics module couples the motor to a battery. Architectures with two motors have been studied in the literature and [3] provides a method for optimizing the torque applied by each motor of a dual motor drive system of an all-electric vehicle. The authors in [4] applied the Pontryagins minimum principle optimization to their dual motor setup. Based on the optimization results, a control strategy is developed which is a combination of mode switching control and power-split control. The research in [5] proposes a brake energy recovery strategy for a dual-motor dual-axis electric powertrain. Their new strategy achieves 9.95% higher regeneration than the front axle braking strategy while keep the same driving behavior. In [6], a novel dual-motor coupling powertrain that couples speed and torque is proposed. Although coupling multiple motors to a driveline could have its own complexity, it is a problem with all HEVs or EVs that incorporate more than one motor or engine and this technology has been well established.

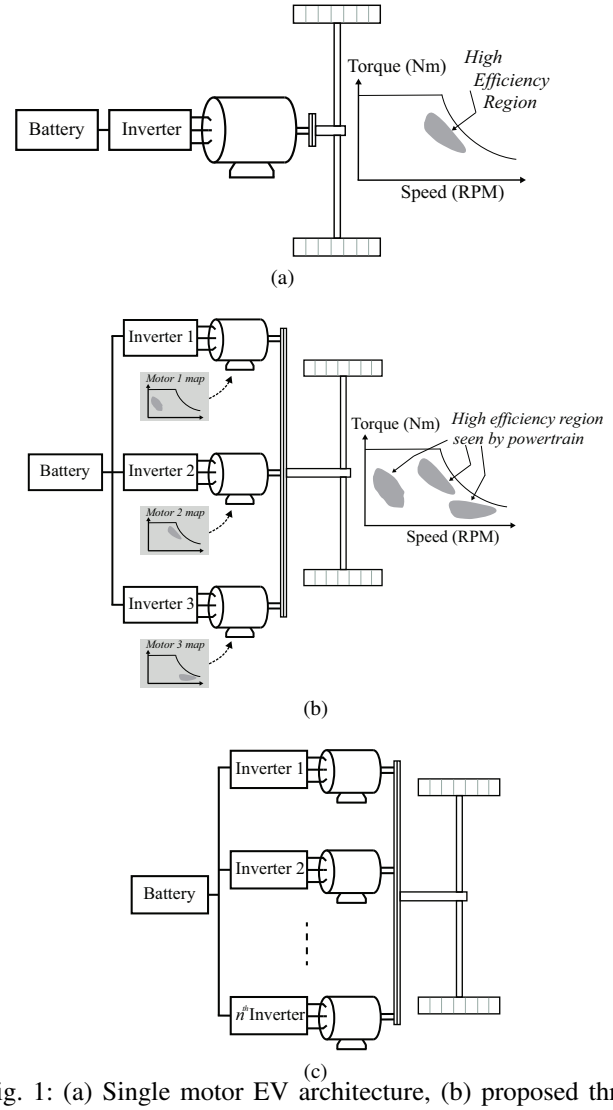

Fig. 1: (a) Single motor EV architecture, (b) proposed three-motor architecture, and (c) proposed multi-motor architecture with n-motors

The coupling of the motors onto a single powertrain will not be the focus of this paper.

Other architectures have incorporated the motors directly on to the wheels. One main advantage of in-wheel motors is the reduction of distance for power transmission which would provide an increase in efficiency. A driving and control system for a direct-wheel-driven EV is proposed in [7], which employs

This is the author's manuscript of the article published in final edited form as:

Nezamuddin, O., Bagwe, R., & Dos Santos, E. (2019). A Multi-Motor Architecture for Electric Vehicles. 2019 IEEE Transportation Electrification Conference and Expo (ITEC), 1–6. https://doi.org/10.1109/ITEC.2019.8790582

two permanent-magnet brushless dc motors (PMBDCMs) and a control strategy that simplifies the commonly complex differential algorithm for steering. In [8], a current distribution control for a dual direct driven wheel motors is proposed. The authors determine the necessary amount of input current to each driving wheel with a load disturbance observer, model following controller and a velocity command compensator. Other control systems have been proposed for an EV with four in-wheel drive systems such as those in [9] and [10]. Although in-wheel drive systems present specific technical advantages, they face considerable challenges. Some of those challenges include limited space to work with, increasing the unsprung weight, and a lack of differential requires a complex torque controller to achieve different wheel speeds [11]. Other notable issues with in-wheel motors include the effects of heat from braking on the motor performance, any shocks and bumps seen on the road by the wheel would affect the motor components connected in the wheel setup. An in-depth review on mechanical causes of failure modes for in-wheel motors in EVs is presented in [12].

This paper proposes an architecture for EVs that incorporates three electric motors with different operating regions to be used for propulsion. The main advantage is that at different speeds and torque demands, a controller can determine which motor would be running based on their efficiency map. This way the motor with maximum efficiency at the current speed will be used for propulsion. Following this section, this paper covers the proposed multi-motor architecture. Then, section 3 will discuss the proposed modeling of the EV followed by the simulation results along with a comparison with other single motor EVs in section 4. Finally, section 5 and 6 will discuss a generalization of the architecture along with a brief conclusion.

II. Proposed Multi-Motor Architecture

A typical architecture of an EV with a single motor is presented in Fig. 1(a). Considering that its a single motor, its efficiency map would have a single region of high efficiency. This means that unless the motor is running at the desired optimal speed and torque, it would be operating in regions that are not considered highly efficient. This paper proposes a multi-motor approach for an EV powertrain shown in Figs. 1(b) and 1(c) with three and n-motors respectively.

In this proposed architecture, three or more different motors, with different operating regions are chosen. This way, a controller can decide which motor to run based on their efficiency map at the demanded torque and speed. This method produces a larger high efficiency region seen by the powertrain, which translates to less losses and consequently improves the SOC.

III. Proposed EV Modeling

There are two globally accepted methods for modeling an EV, a forward-facing powertrain model and a backward-facing powertrain model [13]. The modeling employed in this paper is the forward-facing and was implemented in MATLAB®/Simulink ®. Fig. 2 shows the main block diagram representing the model of a typical EV. The drive cycle data

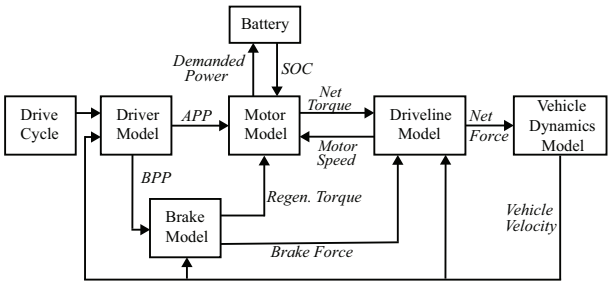

Fig. 2: Block diagram of the proposed EV.

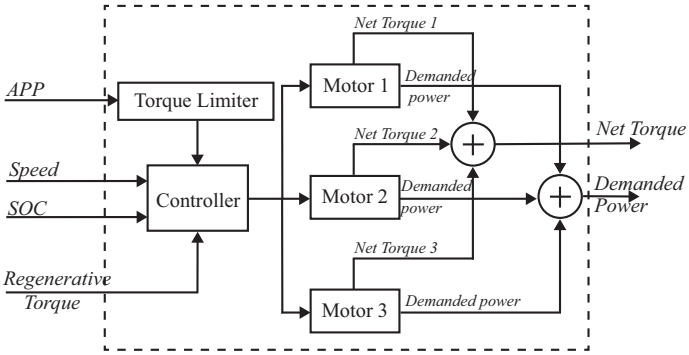

Fig. 3: Block diagram of the motor model with a three-motor configuration.

(reference vehicle speed) is compared with the actual vehicle speed in the driver model block, and the difference (error) is applied to a PID controller to define the accelerator pedal position (APP) along with the brake pedal position (BPP). The APP then goes to the motor block shown with more details in Fig. 3. Herein, the APP requests the amount of torque to reduce the speed difference, but is limited by a one-dimensional lookup table that defines how much maximum torque is allowed at the current motor speed. The output of the limiter is the positive torque needed for traction. The controller then decides which motor would be appropriate to use based off its efficiency map, and requests that power from the battery. Fig. 4 shows a flowchart of the controller logic. The SOC is calculated using the coulomb counting method as shown in [14], which can be re-written as:

$$SOC = SOC(t_0) - \frac{1}{C_{rated}} \int_{t_0}^{t_{final}} I_b dt \qquad (1)$$

where C_{rated} is the rated energy capacity of the battery, t_0 is the initial time, t_{final} is the final time, and I_b is the battery current. The convention here is that positive current I_b is coming from the battery. For a simplified battery model consisting of an internal resistance (R_i) and voltage (V_i) connected in series only, the current I_b is a function of the power output of the battery (P_{batt}), and can be defined as:

$$I_b = \frac{V_i - \sqrt{V_i^2 - 4R_i P_{batt}}}{2R_i} \qquad (2)$$

where $P_{batt} = \frac{1}{\eta} P_{motor}$, η is the efficiency and P_{motor} is the output power of the motor. It is evident that as the efficiency increases, P_{batt} decreases as a result affecting the SOC.

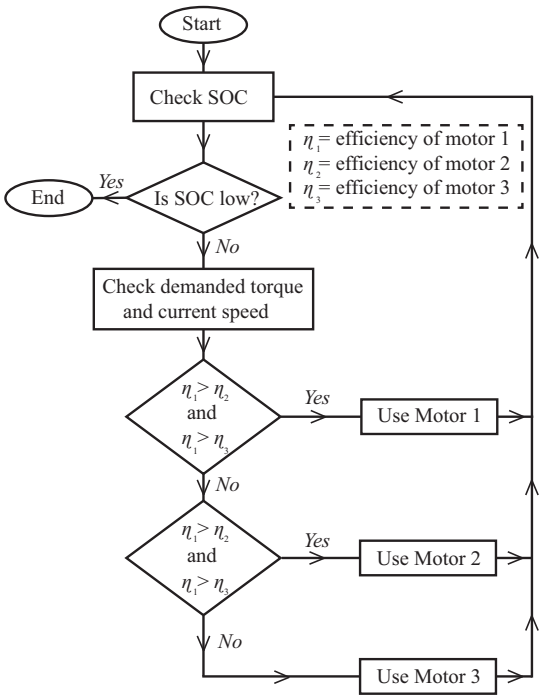

Fig. 4: Flowchart of motor controller.

TABLE I: Vehicle Dynamic Parameters.

Parameter	Value
Air density	1.23 kg/m^3
Drag coefficient	0.38
Vehicle frontal area	2.1 m^2
Vehicle mass	1560 kg
Gravitational acceleration	9.81 m/s^2
Road angle	0 $Degrees$
Rolling resistance coefficient	0.01

The net tractive torque from the motor model is converted to net tractive force in the driveline block, which is sent to the vehicle dynamics model block to obtain the current vehicle speed.

IV. Simulation Results

This section provides a comparison between the proposed methodology and current existing architectures. Figs. 5(a)-5(c) show the maps of three different motors with high efficiency areas on different operating regions. In this section they will be denoted as Motor 1, Motor 2, and Motor 3 respectively. Each motor was simulated separately to see their behaviour with different drive cycles, and then compared with the proposed combined multi-motor architecture. In the combined architecture, since the controller decides which motor to operate, the powertrain views an efficiency map that is the combination of the three motors' maps, shown in Fig. 5(d).

For this simulation, the vehicle dynamics used are presented in Table I. The drive cycles in Figs. 6(a)-6(d) (obtained from [15]) were used to observe the behavior of SOC under

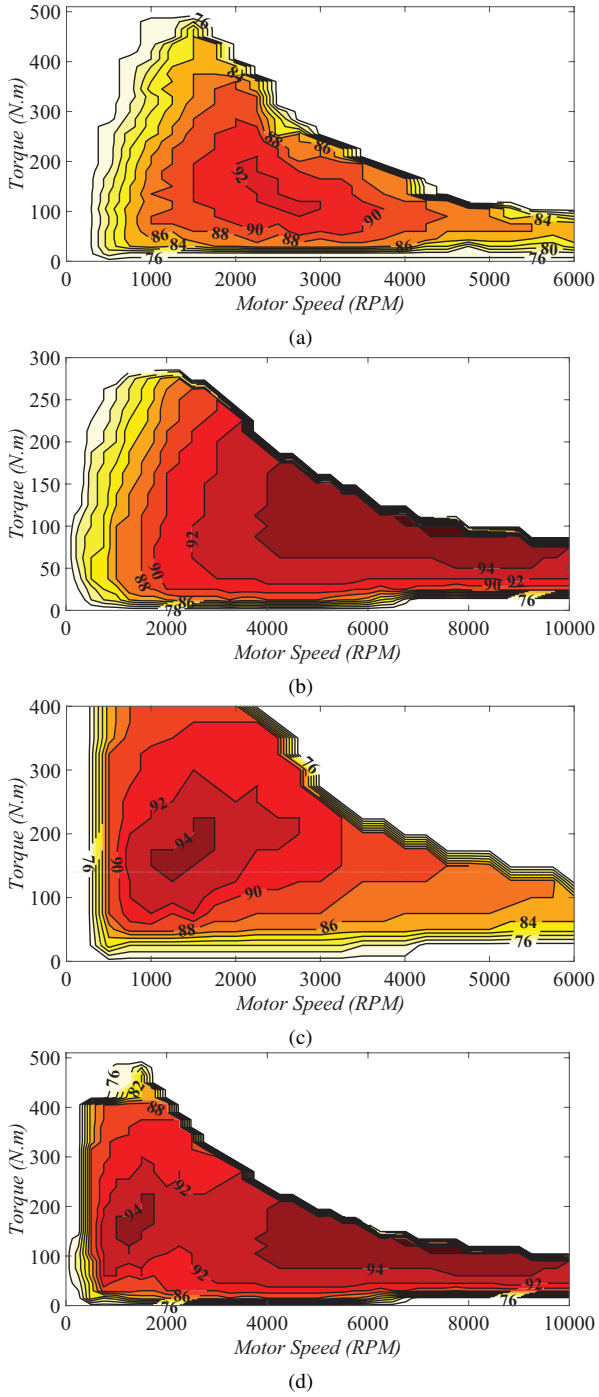

Fig. 5: Motor efficiency maps: (a) motor 1, (b) motor 2, (c) motor 3, and (d) combined motors.

different driving conditions. Fig. 6(a) is a version of the Federal Test Procedure (FTP) drive cycle and it represents city driving conditions followed by a short pause, then repeats the first 505 seconds again. Fig. 6(b) has a portion of the drive cycle known as "Supplemental FTP" (US06) repeated 4 times, which represents a highway drive cycle. Fig. 6(c) is the Urban Dynamometer Driving Schedule (UDDS), and Fig. 6(d) is a combination of Fig. 6(a) and 6(b). Figs. 7(a)-7(d) shows the compared battery's SOC for each drive cycle, and

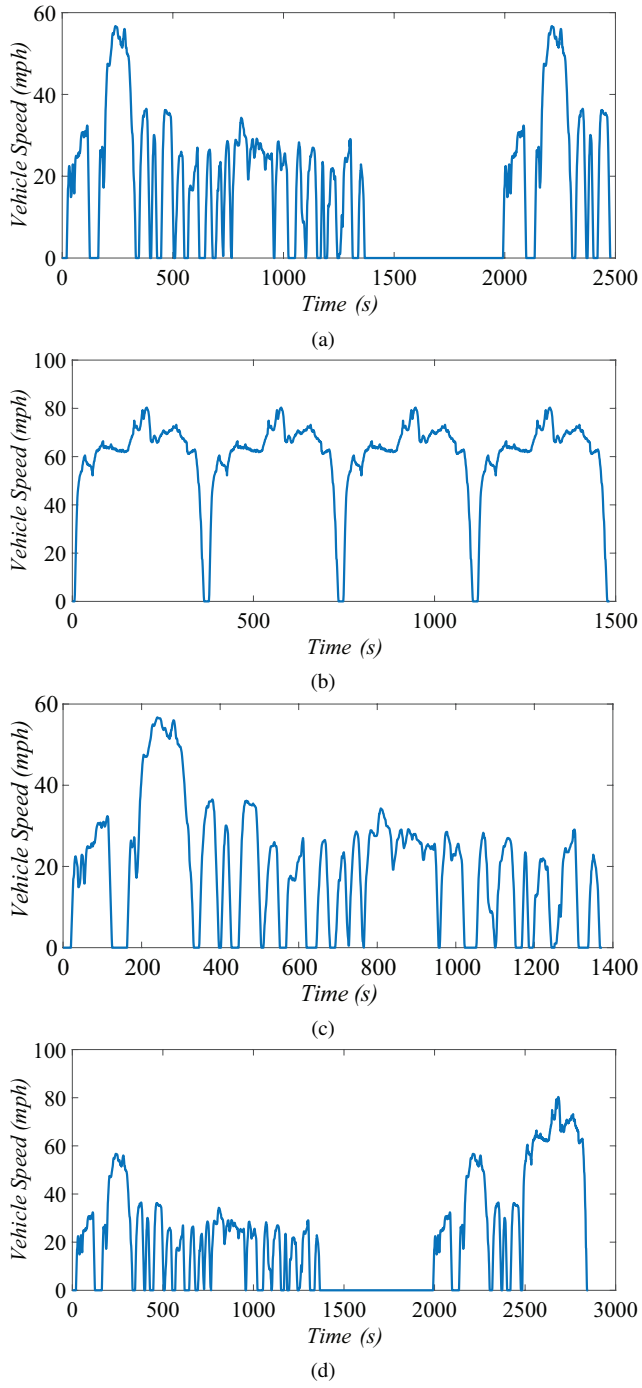

Fig. 6: Drive cycles compared: (a) FTP, (b) US06Hwy (repeated), (c) UDDS, and (d) a combined FTP and US06Hwy.

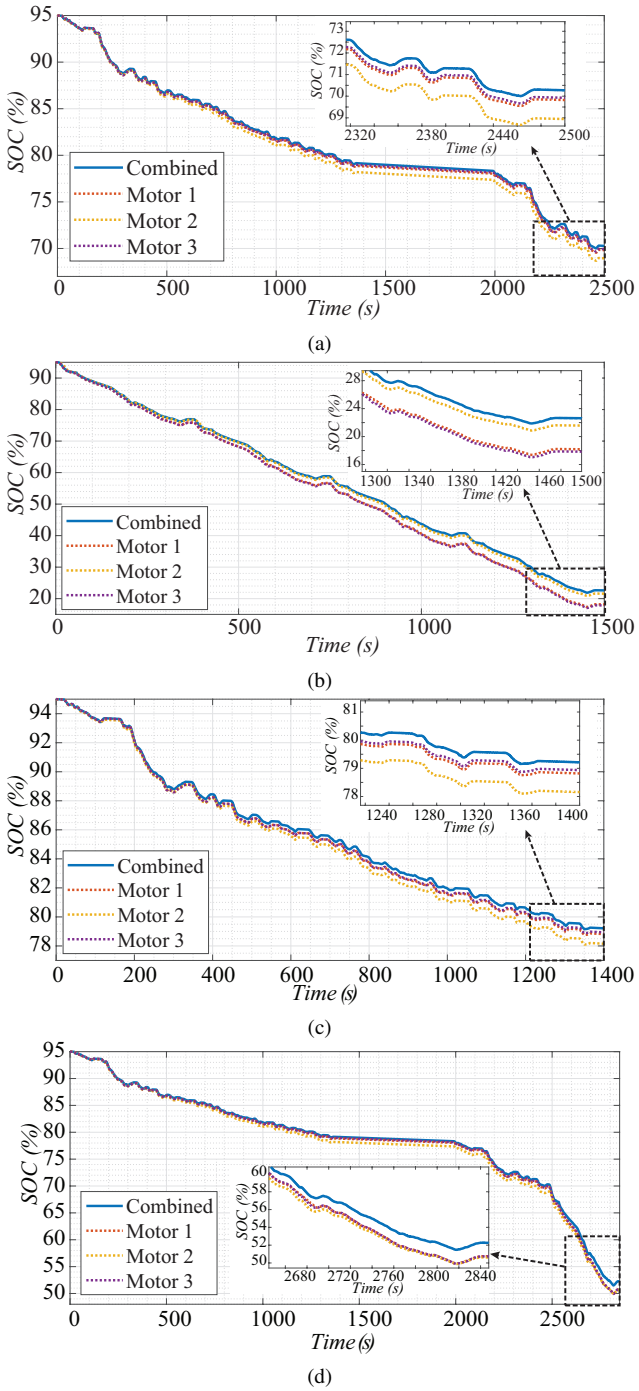

Fig. 7: SOC for (a) FTP, (b) US06Hwy, (c) UDDS, and (d) the combined FTP and US06Hwy drive cycle.

Figs. 8(a)-8(d) are the operating regions for those drive cycles respectively. It can be seen that the proposed architecture performs better in all cases, which translates to longer range for the same given battery capacity.

The first drive cycle tested was the FTP drive cycle. The corresponding Fig. 7(a) shows that after 2500 seconds, the proposed multi-motor architecture has an SOC that is approximately 0.4% higher than Motor 3, 0.6% higher than Motor 1, and 1.5% higher than Motor 2. Although the operating region of this drive cycle (Fig. 8(a)) has a majority that is well within the high efficient region of Motor 3 and Motor 1, the proposed motor will incorporate those regions in which Motor 2 is more efficient hence producing higher SOC levels. The second drive cycle focused mainly on highway driving conditions. The test was repeated 4 times to observe the effects of longer highway drives on the SOC when comparing the four configurations. Herein (Fig. 7(b)), after 1500 seconds, the proposed multi-motor architecture is about 1.1% higher than

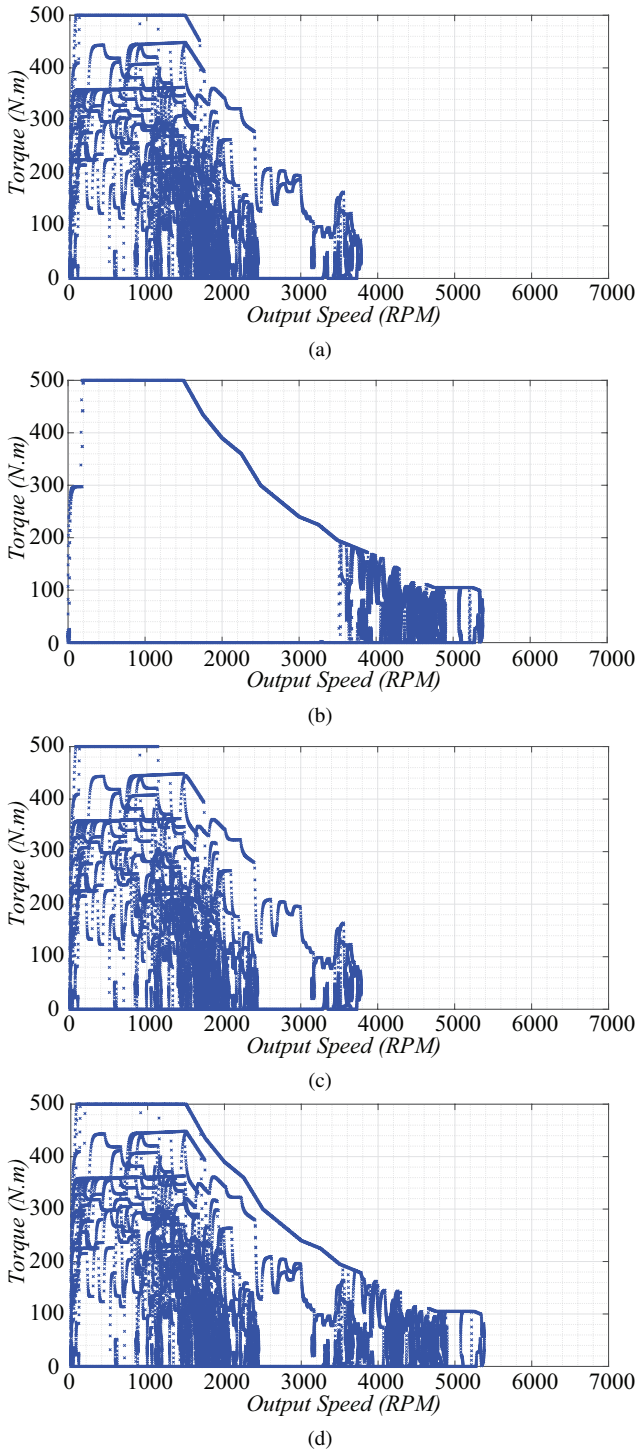

Fig. 8: SOC for (a) FTP, (b) US06Hwy, (c) UDDS, and (d) the combined FTP and US06Hwy drive cycle.

Motor 2, 4.4% higher than Motor 1, and 4.8% higher than Motor 3. By observing Fig. 8(b), it can be seen that Motor 2 would also do a good job in terms of SOC since it is most efficient at higher speeds. The third drive cycle tested was the well known UDDS, which observes the behaviour of typical city driving conditions. It can be seen from Fig. 7(c) that after 1400 seconds the proposed architecture has an SOC that is

TABLE II: Battery SOC Comparison.

Drive Cycle	Motor 1	Motor 2	Motor 3	Three Motors
FTP	69.7%	68.8%	69.9%	70.3%
US06	18.2%	21.5%	17.8%	22.6%
UDDS	78.8%	77.7%	78.9%	79.2%
Mixed	50.7%	50.6%	50.7%	52.3%

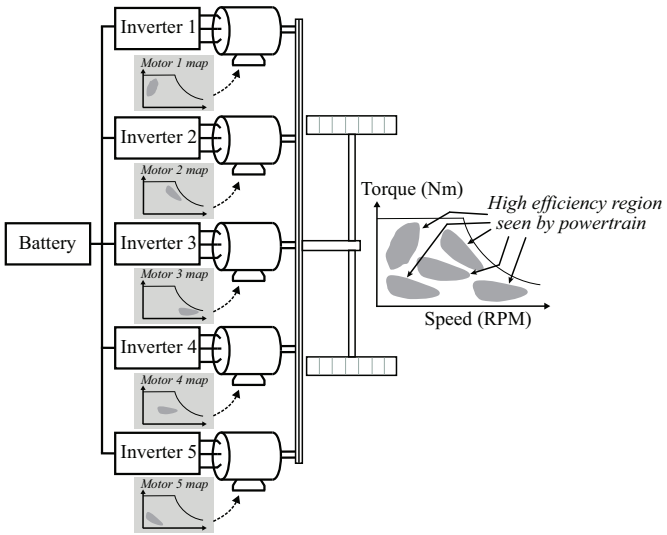

Fig. 9: Multi-motor architecture with 5 motors.

0.25% higher than Motor 3, 0.4% higher than Motor 1, and 1.5% higher than Motor 2. Fig. 8(c) shows the operating region of this drive cycle is similar to that of the first test, hence similar results in terms of SOC performance. The final drive cycle tested was a combination of the FTP and US06. It is clear in Fig. 7(d) that after 2848 seconds, the proposed architecture has an SOC that is 1.6% better than Motor 1 and 3, and 1.7% better than Motor 2. Looking at the operating regions of this mixed drive cycle shown in Fig. 8(d), it is evident that it is a combination of the other three drive cycles. The proposed architecture will always choose the motor with the highest efficiency at the current operating region, thus providing higher SOC levels. Table II shows the SOC of the battery at the end of the aforementioned drive cycles.

V. Generalized Architecture

The multi-motor architecture proposed in this paper incorporates motors with different high efficiency operating regions. As the number of motors increase, the high efficiency region seen by the powertrain becomes larger. Fig. 9 shows a set up of five motors, with a corresponding map seen by the powertrain shown in Fig. 10(a). Although the efficiency map can still be improved with more motors, the results indicate that there is no tangible difference in efficiency after five motors. Fig. 10(b) highlights this by comparing the SOC of a three-motor, five-motor, and a n-motor architecture. Herein, the difference between a three-motor and a five-motor configuration after

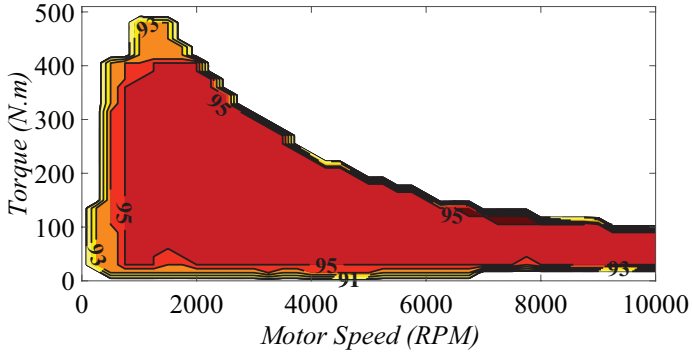

(a)

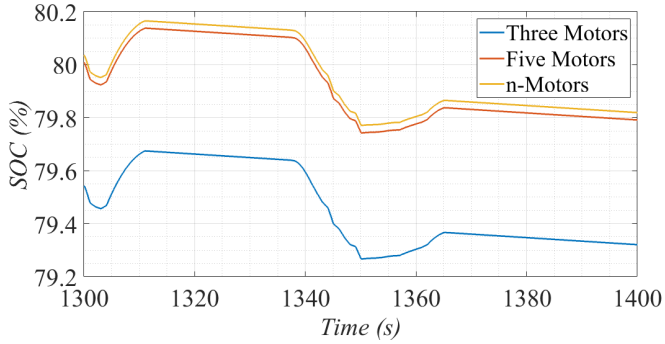

(b)

Fig. 10: (a)An n-motor efficiency map. (b) SOC of 3 motors, 5 motors, and n-motors

1400 seconds is about 0.47%, whereas the difference between the five-motor and n-motor configuration is about 0.03%. In this case, the n-motor architecture map was assumed with a minimum efficiency of 90% and a majority of 95% across the entire torque-speed region.

VI. Conclusion

In EVs with single motor setups (or dual motors of the same kind), the motor operates at its highest efficiency only at a certain region of speed and torque. This paper introduced a multi-motor architecture for EVs that incorporates motors with different high efficiency operating regions. Based on the current vehicle speed and demanded torque, a controller decides which motor would be most efficient to run for the given operating condition. With this architecture, the powertrain sees a combined efficiency map that incorporates the best of each motor. This offers more range for an EV with the same battery capacity when compared to other architectures.

References

[1] A. Zia, "A comprehensive overview on the architecture of hybrid electric vehicles (hev)," in *2016 19th International Multi-Topic Conference (INMIC)*, Dec 2016, pp. 1–7.

[2] H. L. Husted, "A comparative study of the production applications of hybrid electric powertrains," in *Future Transportation Technology Conference & Exposition*. SAE International, jun 2003. [Online]. Available: https://doi.org/10.4271/2003-01-2307

[3] Y. Tang, "Dual motors drive and control system for an electric vehicle." Jun. 2013, U.S. Patent 8453770B2.

[4] S. Zhang, R. Xiong, and C. Zhang, "Pontryagins minimum principle-based power management of a dual-motor-driven electric bus," *Applied energy*, vol. 159, pp. 370–380, 2015.

[5] H. Xiong, X. Zhu, and R. Zhang, "Energy recovery strategy numerical simulation for dual axle drive pure electric vehicle based on motor loss model and big data calculation," *Complexity*, vol. 2018, 2018.

[6] M. Hu, J. Zeng, S. Xu, C. Fu, and D. Qin, "Efficiency study of a dual-motor coupling ev powertrain," *IEEE Transactions on Vehicular Technology*, vol. 64, no. 6, pp. 2252–2260, June 2015.

[7] P. Xu, G. Guo, J. Cao, and B. Cao, "A novel fore axle whole-turning driving and control system for direct-wheel-driven electric vehicle," in *2008 IEEE International Conference on Automation and Logistics*, Sep. 2008, pp. 705–709.

[8] Y.-P. Yang and C.-P. Lo, "Current distribution control of dual directly driven wheel motors for electric vehicles," *Control Engineering Practice*, vol. 16, no. 11, pp. 1285–1292, 2008.

[9] S. D. Pinto, P. Camocardi, A. Sorniotti, P. Gruber, P. Perlo, and F. Viotto, "Torque-fill control and energy management for a four-wheel-drive electric vehicle layout with two-speed transmissions," *IEEE Transactions on Industry Applications*, vol. 53, no. 1, pp. 447–458, Jan 2017.

[10] S. Sakai, H. Sado, and Y. Hori, "Motion control in an electric vehicle with four independently driven in-wheel motors," *IEEE/ASME Transactions on Mechatronics*, vol. 4, no. 1, pp. 9–16, March 1999.

[11] "The pros and cons of using in-wheel motors in electric cars," https://www.plugincars.com/pros-and-cons-wheel-motors-127174.html, accessed: 9- Dec- 2018.

[12] M. Biek, G. Gotovac, D. Miljavec, and S. Zupan, "Mechanical failure mode causes of in-wheel motors," *Strojniki vestnik - Journal of Mechanical Engineering*, vol. 61, no. 1, pp. 74–85, 2015. [Online]. Available: https://www.sv-jme.eu/article/mechanical-failure-mode-causes-of-in-wheel-motors/

[13] G. Mohan, F. Assadian, and S. Longo, "Comparative analysis of forward-facing models vs backwardfacing models in powertrain component sizing," in *IET Hybrid and Electric Vehicles Conference 2013 (HEVC 2013)*, Nov 2013, pp. 1–6.

[14] S. Pickenhain and A. Burtchen, "Optimal energy control of hybrid vehicles," in *Modeling, Simulation and Optimization of Complex Processes HPSC 2015*. Springer, 2017, pp. 179–188.

[15] "Dynamometer drive schedules," https://www.epa.gov/vehicle-and-fuel-emissions-testing/dynamometer-drive-schedules, accessed: 10- Jan- 2019.